# Metal-dioxidoterephthalate MOFs of the MOF-74 type: microporous basic catalysts with well-defined active sites

Pieterjan Valvekens,[a] Matthias Vandichel,[b] Michel Waroquier,[b] Veronique Van Speybroeck[b]* and Dirk De Vos[a]*

[a] Centre for Surface Chemistry and Catalysis, University of Leuven, Kasteelpark Arenberg 23, box 2461, 3001 Leuven, Belgium. [b] Center for Molecular Modeling, Universiteit Gent, Technologiepark 903, 9052 Zwijnaarde, Belgium. * Corresponding authors: veronique.vanspeybroeck@ugent.be; dirk.devos@biw.kuleuven.be

**Keywords**

Metal-organic framework, CPO-27/MOF-74, basic catalysis, Knoevenagel condensation, Michael addition, phenolate oxygen

**Abstract**

The hybrid frameworks $M_2$dobdc (dobdc$^{4-}$ = 2,5-dioxidoterephthalate, $M^{2+}$ = $Mg^{2+}$, $Co^{2+}$, $Ni^{2+}$, $Cu^{2+}$ and $Zn^{2+}$), commonly known as CPO-27 or MOF-74, are shown to be active catalysts in base-catalyzed reactions such as Knoevenagel condensations or Michael additions. Rather than utilizing N-functionalized linkers as a source of basicity, the intrinsic basicity of these materials arises from the presence of the phenolate oxygen atoms coordinated to the metal ions. The overall activity is due a complex interplay of the basic properties of these structural phenolates and the reactant binding characteristics of the coordinatively unsaturated sites. The nature of the active site and the order of activity among the different $M_2$dobdc materials were rationalized via computational efforts; the most active material, both in theory and experiment, is the Ni-containing variant. The basicity of $Ni_2$dobdc was experimentally proven by chemisorption of pyrrole and observation by IR spectroscopy.

## 1. Introduction

Metal-organic frameworks (MOFs) have attracted much interest due to their large compositional and structural diversity. A myriad of applications have been investigated so far, in domains like gas storage, separations and catalysis.[1-3] The exploration of the catalytic potential of MOFs however has mainly focused on acid or redox catalysis. Reports on the catalytic activity of MOFs in base-catalyzed reactions are much more scarce, and the reported materials can be divided into two groups. A first group consists of porous materials containing N-functionalized ligands, e.g. aminoterephthalic acid.[4-7] In these materials, the N-functionality acts as the basic catalytic site. The relatively weak basicity of these sites however, with electron withdrawing carboxylic groups on the same aromatic ring, limits the reaction scope of these catalysts, and some of the early reports, e.g. on amino-substituted MOF-5, have been reinterpreted in terms of structural defects of water-labile Zn frameworks.[8] The second group of materials comprises structures lacking the porosity requirements for intraporous catalysis, featuring basic sites mainly at lattice terminating surface sites. Examples of such materials are the Zn-imidazolates ZIF-8 and ZIF-9,[9-11] in which the pore windows are too narrow to allow diffusion of most reactants and/or products, or a Ba-3,5-pyrazoledicarboxylate MOF having a limited microporous volume ($S_{BET}$= 56 m²/g).[12] If catalysis is confined to the outer surface, the catalytic material is used only for a very limited fraction, and the precise nature of the sites at the surface is not always well defined. The group of Koner also synthesized and used various MOFs combining Mg or Ba and pyrazole-3,5-dicarboxylic acid or pyridine-2,5-dicarboxylic acid.[13-15] Although these materials were catalytically active in aldol condensation reactions, the presence of stoichiometric amounts of the base triethylamine was required to obtain sufficient reaction rates.

To the best of our knowledge, there are no studies of porous MOFs with an intrinsic framework basicity that are useful in classical base-catalyzed reactions such as Knoevenagel condensations or conjugate additions. We here report that surprisingly, $M_2$dobdc type MOFs are active catalysts for such reactions, with intrinsically basic properties. $M_2$dobdc represents a series of isostructural compounds, denominated CPO-27-M by Dietzel *et al*.,[16-20] or MOF-74 for the zinc compound by

Rosi *et al.* [21] (CPO: Coordination Polymer of Oslo; M = Ni, Co, Zn, Mg, Mn). The structure consists of metal oxide chains connected by the 2,5-dioxidoterephthalate linker ($dobdc^{4-}$) forming a honeycomb-like structure with large, one-dimensional hexagonal pores of 1.1-1.2 nm in diameter (Figure 1(top)). In Figure 1 (bottom) the potentially available base sites in the framework are displayed, together with the well-known coordinatively unsaturated sites.[22]

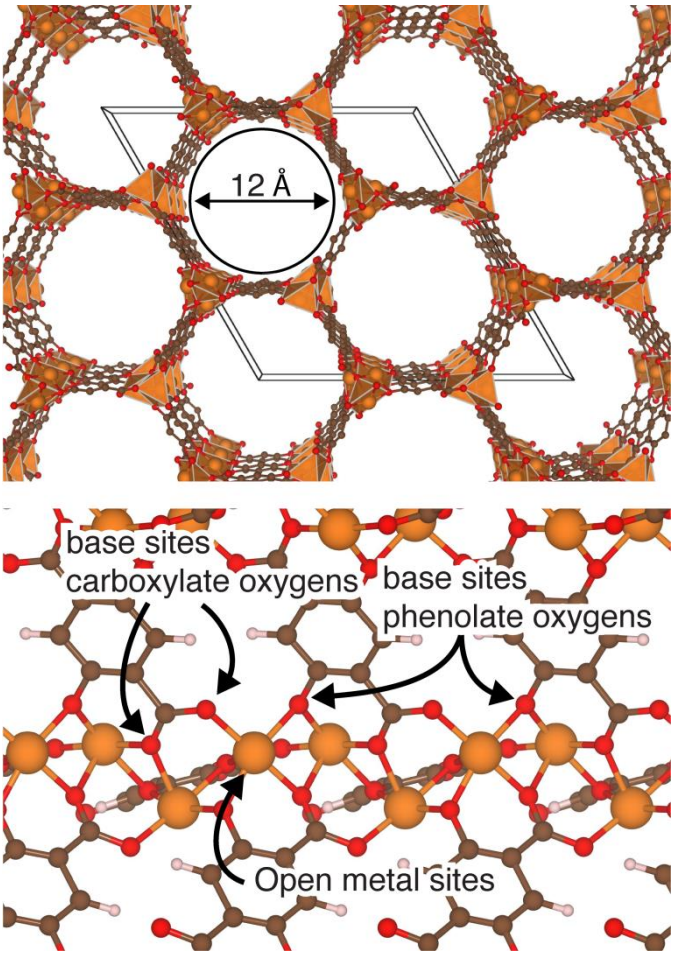


**Figure 1.** (top) Pores in the $M_2dobdc$ MOF; a sphere with a diameter of 1.2 nm fits inside the pores (brown = carbon; orange = metal; red = oxygen); (bottom) Representation of the potential base sites and open metal sites in the framework.

The high density of exposed metal ions in these materials has sparked much interest in the field of adsorption and the adsorptive separation of compounds such as CO, $CO_2$, $CH_4$, ethane, acetylene, propane, propylene or $H_2S$.[20, 23-31] The existence of a family of isostructural materials has also

allowed to study the specific role of the metal ion in these adsorption processes.[20, 24, 29, 32] Reports of catalysis using $M_2$dobdc are very limited hitherto; they focus on the role of the metal ion as a Lewis acid center, or in accelerating autoxidation reactions.[22, 33, 34] The present study focuses on the use of the $Mg^{2+}$, $Co^{2+}$, $Ni^{2+}$, $Cu^{2+}$ and $Zn^{2+}$ variants as catalysts in Knoevenagel condensation and Michael conjugate addition reactions, and on understanding the activation of the reactants on the phenolate-metal active sites. The successful application of these MOFs for these standard base catalyzed reactions, opens a new window for catalysis research using the intrinsic basicity of MOFs.

## 2. Materials and methods

### 2.1 Materials

Copper(II) nitrate trihydrate, malononitrile and 2-cyclohexene-1-one were purchased from Fluka; *N*,*N*-dimethylformamide, *N*-methylpyrrolidone, zinc nitrate hexahydrate, benzaldehyde and 2-cyclopentene-1-one from Acros; methanol, toluene and acetonitrile from VWR; magnesium acetate tetrahydrate, ethyl cyanoacetate, ethyl acetoacetate and acetophenone from Aldrich; tetrahydrofuran and methyl vinyl ketone from Sigma Aldrich; cobalt nitrate hexahydrate from Alfa Aesar; nickel acetate tetrahydrate, diethyl malonate, cyclopentanone and cyclohexanone from Janssen Chimica and 2,5-dihydroxyterephthalic acid from TCI. All chemicals were of the highest grade available and were used without further purification.

### 2.2 Catalyst preparation

$Mg_2$dobdc, $Co_2$dobdc, $Ni_2$dobdc, $Cu_2$dobdc and $Zn_2$dobdc were synthesized according to literature procedures.[26, 35-37] The synthesis solvent was removed by washing the material seven times with methanol over a period of four days. Prior to catalytic testing, the materials were activated under vacuum, < $10^{-5}$ bar, at elevated temperature according to literature procedures, i.e. 130°C, 200°C,

240°, 250°C and 270°C for $Cu_2$-, $Mg_2$-, $Ni_2$-, $Co_2$- and $Zn_2$dobdc respectively. After activation, the materials were transferred under inert conditions to the reaction vessel.

### 2.3 Catalyst characterization

The crystallinity of the synthesized materials was confirmed via powder X-ray diffraction (PXRD). Reflection patterns were recorded on a STOE STADI MP in Bragg-Brentano mode (2θ - θ geometry; CuKα1, 1.54060 Å) using a linear position sensitive detector. $N_2$ sorption measurements were performed on a Micromeritics 3Flex surface analyser at 77 K. Prior to measurements, the samples were activated under vacuum at the temperatures reported in literature (*vide supra*). Fourier transform infrared spectroscopy measurements (FTIR) were performed on a Nicolet 6700 spectrometer. Thin self-supporting wafers (± 10 mg $cm^{-2}$) were prepared and introduced in an *in situ* cell. The cell was brought under vacuum ($p < 10^{-4}$ Pa) at 240°C and IR spectra of the evacuated sample were recorded at different temperatures during the subsequent cooling period. Pyrrole was adsorbed at room temperature from the vapour and the weakly physisorbed pyrrole was evacuated at 50°C, after which the spectrum was recorded and compared with the spectrum of the original sample at 50°C.

### 2.4 Catalyst evaluation

In a typical reaction, 1 mmol of each reactant was combined with 2 ml of solvent, toluene for the Knoevenagel condensations or acetonitrile in the Michael addition. The mixture was added to 50 mg of activated catalyst. The reaction mixture was heated to 70°C and aliquots of sample were removed for analysis at set intervals. The identity of the reaction products was verified by GC-MS (Agilent 6890 gas chromatograph, equipped with a HP-5MS column, coupled to a 5973 MSD mass spectrometer) and the product yields were determined via GC-analysis. The substrate scope was evaluated in reactions in which 1 mmol of each reactant was combined with 2 ml of toluene. This mixture was added to 50 mg of appropriately activated $Ni_2$dobdc and stirred at 110°C.

## 2.5 Theoretical modeling

The theoretical part of this study focuses on the key steps initiating the Knoevenagel condensation reactions, in an attempt to understand the order of activity as observed experimentally for the different $M_2$dobdc materials. In order to get a first vision on the basicity of the material and on the characteristics of the open metal sites, a preliminary study has been performed by evaluating the proton affinities of the pristine nanoporous materials and their adsorption properties with respect to some small probe molecules.

Periodic DFT-D calculations were carried out on all $M_2$dobdc structures (M = Co, Ni, Cu, Mg, Zn) with the Vienna Ab Initio Simulation Package (VASP 5.2.12).[38-41] For each metal, a 2x1x1 unit cell was optimized with a plane wave kinetic energy cutoff of 550 eV, employing the PBE exchange-correlation functional [42, 43] with D2-dispersion corrections of Grimme and coworkers [44], followed by a single point energy computation at the PBE-D3 level of theory. The projector augmented wave approximation (PAW) [45] was used. Brillouin zone sampling was restricted to the Γ-point. Gaussian smearing [39] was applied to improve convergence: 0.05 eV for cell optimizations and energy calculations. For the cell optimizations, the convergence criterion for the electronic self-consistent field (SCF) problem was set to $10^{-6}$ eV while the atomic forces were converged below 0.01 eV/ Å (structures are reported in Supporting Information). For the further applications the cell parameters were kept fixed; the kinetic energy cut off was lowered to 400 eV, and the atomic force criterion was set on 0.03 eV/Å (for the adsorption and deprotonation reactions). Furthermore, we used spin polarization throughout all calculations applying the most stable spin state for the metal in gas phase for every metal atom in the crystal. The reported adsorption and deprotonation energies do not include Zero-Point Vibrational energies or thermal corrections.

In a first exploratory survey of the nature of the active site, adsorption energies of some basic probe molecules on the coordinatively unsaturated sites (cus) were calculated. Herefore, we used the methodology as outlined above for the periodic structure calculations. Another bulk property, which

is indicative for the base strength, is the proton affinity of the material (PA). Periodic calculations fail in reproducing accurate proton affinities or deprotonation energies of periodic materials, due to the charge of the proton induced in the unit cell when adding or removing a proton from the framework; therefore cluster calculations were preferred. The cluster models were cut from the optimized periodic structures (see Figure S.2), which in turn are further optimized with the Gaussian09 package, [46] using the B3LYP hybrid functional [47, 48] including D3 Grimme corrections for the van der Waals interaction. [44] The double-zeta Pople basis set 6–31g(d) was used for all atoms. By fixing the outer carboxyl oxygen atoms, we maintained the rigidity of the cluster model as in the crystal. The manipulation of the periodic structure files and the cluster models was performed using ZEOBUILDER, an in house developed software tool for building complex molecular structures. [49] Partial Hessian Vibrational Analysis has been post-processed using the program TAMKIN.[50]

## 3. Results and Discussion

### 3.1 Activity of $M_2$dobdc materials with various structural cations

All materials were synthesized and pretreated according to literature procedures and PXRD patterns and BET surface areas of the synthesized materials can be found in Figure S1. Knoevenagel condensations are widely studied for MOFs and some excellent catalysts have already been reported. These range from purely basic MOFs with N-functionalized groups,[4, 9, 51] to MOFs featuring Lewis acid active sites such as $Cu_3(BTC)_2$, $Fe_3(BTC)_2$ or $Ni_4(MTB)_2$ ($H_3BTC$ = trimesic acid, $H_4MTB$ = methanetetrabenzoic acid) .[52-55] The catalytic activity of $M_2$dobdc in some typically base catalyzed reactions was therefore first evaluated via the Knoevenagel condensation of malononitrile (MN) and benzaldehyde (BA) (as shown in Scheme 1), and of ethyl cyanoacetate (ECA) and benzaldehyde. In order to take into account the lower atomic weight of magnesium compared to the transition metal ions tested, the amount of $Mg_2$dobdc used in these tests was adapted accordingly. The catalytic data (Table 1) show a distinct influence of the metal ion on the performance of the catalyst, with a clear

preference for $Ni_2$dobdc (entry 3) as the most active material in the reaction of MN and BA. These trends are based on initial rates ($X_{2h}$), which should be only minimally affected by the possible adsorption of the reaction products. For the MN + BA Knoevenagel condensation we found experimentally an overall order of activity of Ni > Cu > Mg ~ Zn > Co. Replacing MN by the more weakly acidic ECA as donor, the conversion occurs significantly more slowly and after 2 h no clear discrimination between the yields over the various catalysts can be extracted. Very roughly we found following order of activity: Ni ~ Mg ~ Zn > Co ~ Cu (see Table 1). The lower reactivity of ECA vs. MN was also observed in other catalytic studies.[54, 56, 57]

**Table 1.** Conversion (*X*) measured after 2 and 24 h of reaction for the different $M_2$dobdc materials in Knoevenagel condensation and Michael addition reactions.[a]

| | | Knoevenagel condensation MN + BA | | Knoevenagel condensation ECA + BA | | Michael Addition ECA + MVK | |
|---|---|---|---|---|---|---|---|
| | M | $X_{2h}$ | $X_{24h}$ | $X_{2h}$ | $X_{24h}$ | $X_{2h}$ | $X_{24h}$ |
| *1* | Mg | 17 | 73 | 3 | 14 | 6 | 35 |
| *2* | Co | 4 | 32 | 0 | 9 | 9 | 42 |
| *3* | Ni | 69 | 99 | 3 | 9 | 26 | 66 |
| *4* | Cu | 39 | 69 | 0 | 9 | 13 | 38 |
| *5* | Zn | 13 | 77 | 3 | 14 | 19 | 44 |

[a] Reaction conditions: 1 mmol of each reactant; 2 ml solvent, 343 K, 50 mg of $M_2$dobdc material (M = Co, Ni, Cu, Zn) or 37 mg (M = Mg); MN = malononitrile, BA = benzaldehyde; ECA = ethyl cyanoacetate; MVK = methyl vinyl ketone.

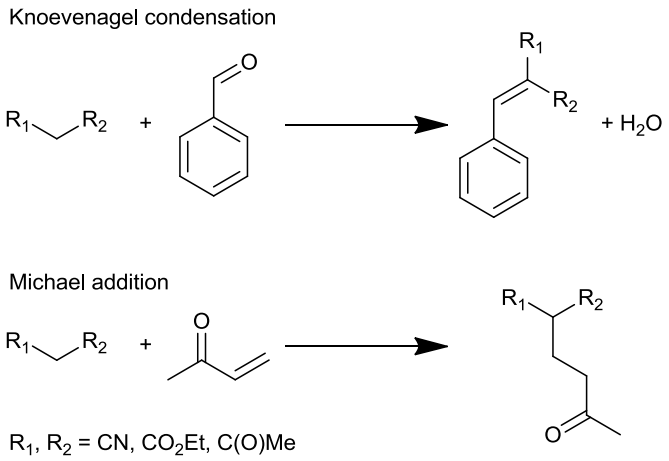


**Scheme 1**

To investigate whether similar activity trends can be observed in other base-catalyzed reactions, an additional Michael addition of ethyl cyanoacetate to methyl vinyl ketone (Scheme 1) was attempted with the same series of catalysts (Table 1). Despite the relatively weak acidity of ethyl cyanoacetate, high conversions are observed, with again the Ni variant as the most active member of the catalyst series.

### 3.2 Detailed study of reactions with the $Ni_2$dobdc catalyst

In view of its high activity, the $Ni_2$dobdc catalyst was employed for studying the reactivity of different starting compounds, in an attempt to obtain more insight in how the reactants are activated. To this end, both the Knoevenagel condensation and the Michael addition reactions were performed in toluene at 110 °C. In the Knoevenagel condensations with benzaldehyde (Table 2), active methylene compounds were tested with p$K_a$ values ranging between 11.1 and 16.4. When varying the donor molecules, their p$K_a$ is clearly decisive for the conversion rates (entries 1 – 4); the highest conversion was observed for the most acidic compound, MN, while both ethyl acetoacetate and diethyl malonate show much lower conversions. Variation of the acceptor molecules shows that the presence of a methyl substituent on the carbonyl group, like in acetophenone, decreases the reactivity of this molecule, which is probably due to steric hindrance (entry 5). Reactions with

cyclopentanone and cyclohexanone (entries 6 and 7) demonstrate the possibility to use also cyclic aliphatic ketones as reactants in Knoevenagel condensation reactions catalyzed by $Ni_2$dobdc.

**Table 2.** Evaluation of the substrate scope for Knoevenagel condensation reactions with $Ni_2$dobdc.[a]

| | Donor (p$K_a$ in DMSO) | | Acceptor | *t*, h | $X_{acceptor}$, % |
|---|---|---|---|---|---|
| *1* | malononitrile | (11.1) | benzaldehyde | 24 | 100 [b] |
| *2* | ethyl cyanoacetate | (13.1) | benzaldehyde | 24 | 25 |
| *3* | ethyl acetoacetate | (14.3) | benzaldehyde | 24 | 3 |
| *4* | diethyl malonate | (16.4) | benzaldehyde | 24 | < 1 |
| *5* | malononitrile | (11.1) | acetophenone | 24 | 13 |
| *6* | malononitrile | (11.1) | cyclopentanone | 24 | 52 |
| 7 | malononitrile | (11.1) | cyclohexanone | 24 | 87 |

[a] Standard reaction conditions: 1 mmol of each reactant, 50 mg of catalyst, 2 ml of toluene, 110°C. $X_{acceptor}$ = conversion of the acceptor molecule; [b] Reaction at 70°C.

While the reactivity of the donor molecules in the Knoevenagel condensation is dominated by the p$K_a$ of these molecules, the donor reactivity order in the Michael addition reactions over $Ni_2$dobdc is more complex (Table 3). At first glance there appears to be a reversal in the expected, p$K_a$-based reactivity order: in these Michael reactions, the lowest conversions were observed for the most acidic donor molecule, malononitrile (entry 1), whereas the highest conversion, even after short time, was observed for the not so acidic ethyl acetoacetate (entry 4). The conversion of diethyl malonate, the least acidic compound (entry 5), is however again slightly lower than that of ethyl acetoacetate. In order to explain such reactivity trends, we hypothesize that not only the donor, but also the acceptor could be activated during the Michael reaction. In such a mechanism, a basic site abstracts a proton from the donor molecule, whereas the α,β-unsaturated carbonyl compound could be activated via coordination on an open metal site. However, if the anion is more easily formed from the donor, as for the more acidic donor molecules, or if there is an excess of coordinating nitrile functional groups, like in malononitrile (entry 1), the coordinatively unsaturated sites may be fully

occupied by either carbanions derived from the donor, or by the nitrile groups. Such a coordination may hamper the activation of the acceptor molecule, slowing down the overall reaction. This could explain why malononitrile containing two nitrile functions would give the lowest rate, closely followed by ethyl cyanoacetate. Such site blocking effects are less expected for donor molecules lacking nitrile functions, such as 2,4-pentanedione, ethyl acetoacetate or diethyl malonate (entries 3 to 5). In order to investigate the effect of the presence of nitriles on the conversion, an additional competitive Michael reaction was carried out using both malononitrile and ethyl cyanoacetate as donor molecules. This reaction shows that, whereas the conversion of malononitrile is relatively uninhibited by ethyl cyanoacetate, the conversion of ethyl cyanoacetate is strongly inhibited by the presence of malononitrile in the reaction mixture (Figure 2). Clearly, in such complex competitive reactions, many effects could play a role, e.g. not only differential occupation of the active sites by reactants, intermediates or products, but also different intraporous concentrations when the sorption equilibrium is attained, etc. Such complexity is beyond the scope of the theoretical work later in this paper, which will mainly address the activation of acidic donor molecules on the $M_2$dobdc active sites.

**Table 3.** Evaluation of the substrate scope for Michael addition reactions with $Ni_2$dobdc, using methyl vinyl ketone as the acceptor.[a]

| | Donor (p$K_a$ in DMSO) | | $t$, h | $X_{acceptor}$, % |
|---|---|---|---|---|
| *1* | malononitrile | (11.1) | 2 (24) | 18 (55) |
| *2* | ethyl cyanoacetate | (13.1) | 2 (24) | 32 (75) |
| *3* | 2,4-pentanedione | (13.3) | 2 (24) | 58 (99) |
| *4* | ethyl acetoacetate | (14.3) | 2 (24) | 93 (99) |
| *5* | diethyl malonate | (16.4) | 2 (24) | 66 (86) |

[a] Standard reaction conditions: 1 mmol of donor, 1 mmol of methyl vinyl ketone as acceptor, 50 mg of catalyst, 2 ml of toluene, 110°C.

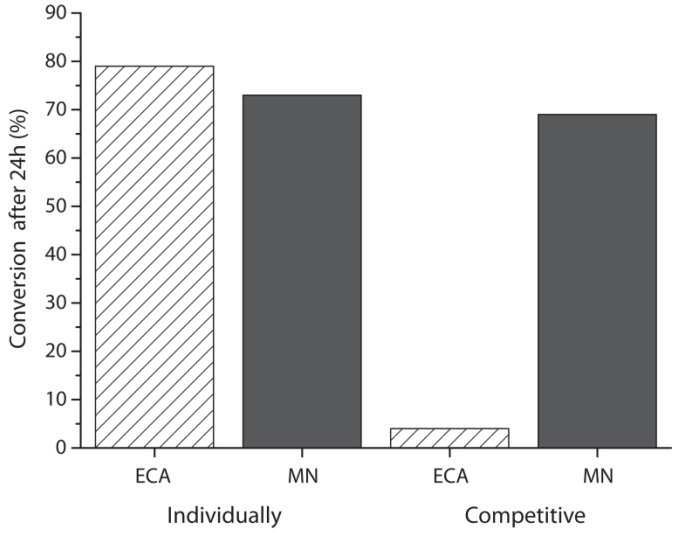


**Figure 2.** Conversion of ethyl cyanoacetate and malononitrile in the Michael addition reaction with methyl vinyl ketone over $Ni_2$dobdc after 24 h, in individual experiments (with one donor) and in a competitive experiment (with two donors). Reaction conditions: 0.5 mmol donor, 1 mmol methyl vinyl ketone, 50 mg of catalyst, 2 ml of toluene, 110°C. In the competitive experiment, 0.5 mmol of each donor molecule and 1 mmol of methyl vinyl ketone was used.

Finally, the reaction between malononitrile and 2-cyclopenten-1-one or 2-cyclohexen-1-one was studied (Table 4). According to literature, the nature of the catalyst strongly influences whether a Knoevenagel or a Michael addition reaction takes place. Whereas Lewis acids such as $RuCl_3$ or Ru-exchanged hydroxyapatite are reported to selectively catalyze the Knoevenagel condensation,[58] bases like 1,1,3,3-tetramethylguanidine [59] or t-BuOK [60] are reported to catalyze the Michael addition reaction of these compounds. Use of $Ni_2$dobdc as a catalyst resulted in the formation of both the Michael addition and the Knoevenagel condensation products (Table 4). In the reaction with 2-cyclopenten-1-one, the Michael addition product is the primary product; with 2-cyclohexen-1-one the main product is the Knoevenagel product. The presence of both the Michael and Knoevenagel reaction products provides evidence for the simultaneous action of base and open metal sites on the catalyst.

**Table 4.** Reactions of 2-cycloalken-1-one acceptors with malononitrile donor using $Ni_2$dobdc catalysts.[a]

| | acceptor | *t*, h | Yield Knoevenagel product, % | Yield Michael product, % | *X*, %[b] |
|---|---|---|---|---|---|
| 1 | 2-cyclopenten-1-one | 24 | 5 | 23 | 27 |
| 2 | 2-cyclohexen-1-one | 24 | 27 | 7 | 35 |

[a] Reaction conditions: 2-cycloalken-1-one (1 mmol), malononitrile (1 mmol), 50 mg $Ni_2$dobdc catalyst, toluene (2 ml), 110°C. [b] Conversion of the acceptor.

The heterogeneity of the $Ni_2$dobdc catalyst was evaluated via a hot filtration test on a Knoevenagel reaction (Figure 3, top). Removal of the catalyst after both 1 and 2 h of reaction, confirms that catalysis is indeed fully heterogeneous. Furthermore, PXRD measurements before and after reaction confirm the stability of the catalyst structure under reaction conditions (Figure 3, middle) and a recycle test confirms that the catalyst can be reused over several runs. Scale-up of a catalytic reaction was successfully performed; using 10 times larger quantities of the reactants and the catalyst than in standard conditions, 1.47 g of $\alpha$-cyanocinnamonitrile (95 % yield) was obtained after 24 h.

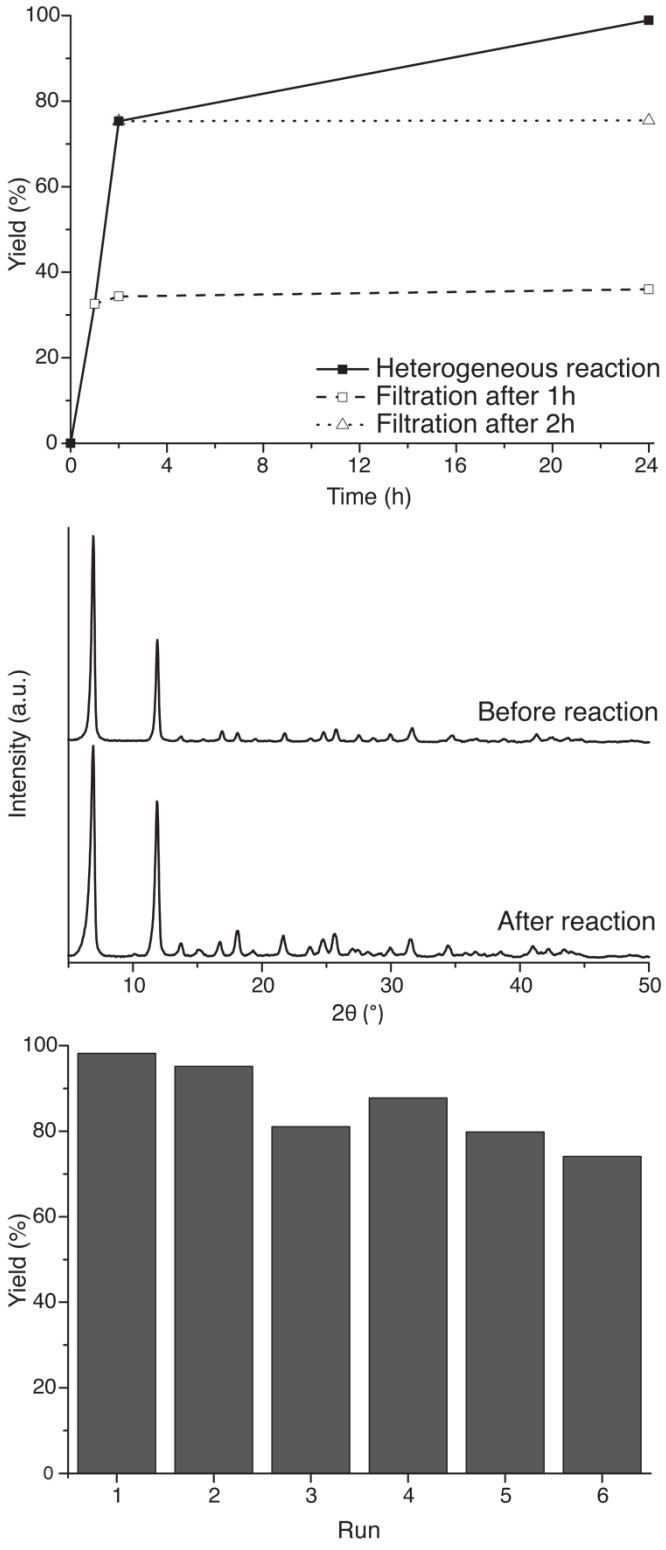


**Figure 3.** Hot filtration test for $Ni_2$dobdc in the Knoevenagel condensation of malononitrile with benzaldehyde (top), PXRD diffraction patterns before and after reaction (middle) and product yield in consecutive runs with the catalyst (bottom).

### 3.3 Spectroscopic observation of the chemisorption of pyrrole

Next, the chemisorption of pyrrole, as an acidic probe molecule, was monitored using FTIR spectroscopy in order to experimentally prove that the $M_2$dobdc materials possess base sites next to the well-known open metal sites. [61-63] Two distinct signals can be observed in the FTIR difference spectrum (Figure 4). A first absorption band at 3405 $cm^{-1}$ typically corresponds to the stretching vibration of the NH group interacting via an NH-π complex with the ring of another pyrrole molecule.[64, 65] The second and most intense absorption band in the diagnostic region of pyrrole can be found for $Ni_2$dobdc at 3253 $cm^{-1}$. Although the exact position of this absorption band can be influenced by different interactions, such as the interaction of the aromatic ring of pyrrole with the open metal site, the strong bathochromic shift of this band compared to that of free pyrrole, is generally attributed to pyrrole species interacting with a H-bond acceptor stronger than pyrrole, for instance a basic site on the surface.[63-65] The shift of the N-H stretching vibration frequency in comparison with that of free pyrrole, at 3500 $cm^{-1}$, is a measure for the basic strength of the adsorption site. A shift of 250 $cm^{-1}$ is comparable to the shift as observed for the interaction of pyrrole with e.g. alumina [65] or pyridine.[64] Similar results were obtained for $Mg_2$-, $Co_2$- and $Zn_2$dobdc; these results are summarized in table S.2 (supporting information).

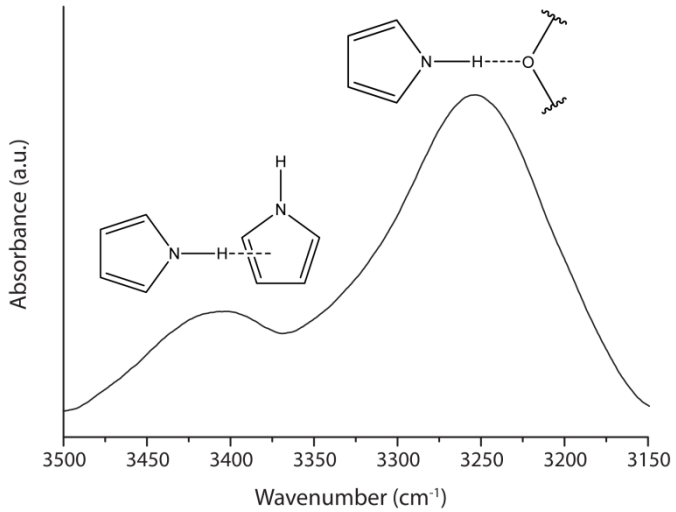

**Figure 4.** FTIR difference spectrum of pyrrole chemisorbed on $Ni_2$dobdc.

Calculation of the N-H stretching frequency in the static mode using periodic code (VASP-PBE-D2) showed that in comparison with free pyrrole, the pyrrole with the N-H oriented towards the phenolate oxygen of $Ni_2$dodbc experiences a 244 $cm^{-1}$ downshift of the stretching frequency, which is in remarkably good agreement with the experimentally observed value. This supports the vision of the phenolate oxygen atom acting as a base towards the pyrrole probe.

### 3.4 Theoretical rationalization of the catalytic activity

The catalytic activity of $M_2$dobdc as a base can be understood by looking at the structure of this MOF. As the linker molecule, 2,5-dihydroxyterephthalic acid, is fully deprotonated in the framework, carboxylate oxygen atoms as well as phenolate oxygen atoms coordinate the metal center (Figure 1(bottom)). While the carboxylate oxygen atoms are only weakly basic, a phenolate oxygen, which is a conjugate base to the weakly acid phenol, is expected to be much more basic. Logically, these phenolate oxygen atoms should act as the basic site in this material, deprotonating the acidic reactant, e.g. malononitrile or ethyl cyanoacetate, thus activating this compound for further reaction. The open coordination site on the metal ion adjacent to the phenolate oxygen atom can act as a docking site for the deprotonated reactant molecule. The second reactant in the Knoevenagel condensation, e.g. benzaldehyde, can be adsorbed on the protonated phenolate oxygen, after which coupling of the reactants takes place as shown in the reaction mechanism displayed in Scheme 2. Such an interplay of metal sites and phenolate oxygen atoms in the formation of acid-base reactive centers in catalysts is similar to what is happening for homogeneous alkaline earth metal binaphtholate catalysts described by e.g. Kobayashi *et al.*[66] or Hatano et al.,[67] for barium and magnesium ions respectively. In the following subsections, molecular modeling will be used for (1) the characterization of the basic sites and the open metal sites in the $M_2$dobdc materials, and (2) studying the initial steps in the reaction mechanism for the Knoevenagel condensation (experimental data in Table 1).

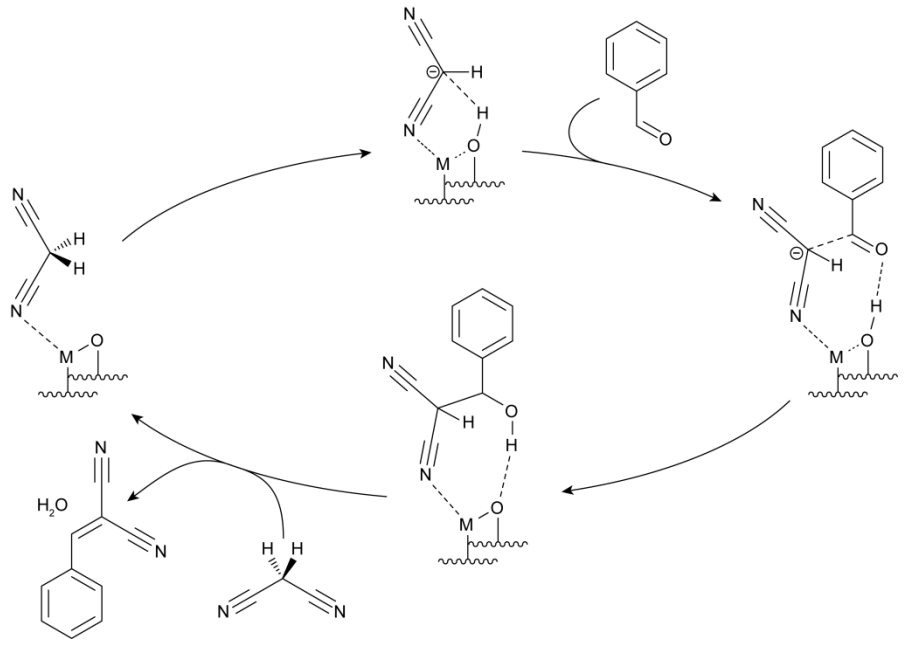

**Scheme 2.** The proposed reaction mechanism for the Knoevenagel condensation of malononitrile and benzaldehyde in $M_2$dobdc

### 3.4.1. The phenolate-metal active site

A priori, one would expect that the basicity of the $M_2$dobdc materials would be affected by the nature of the metal ion $M^{2+}$, as the coordination of the phenolate to the metal ion influences the electron density of the oxygen atom. As a first indication for the basicity of the material, the proton affinity (PA) was calculated in an attempt to explain the experimentally observed conversion order in both the Knoevenagel condensation and Michael addition reactions. PAs were calculated for both the phenolate (PA1) as well as for the carboxylate oxygen atom (PA2) (Figure 1, bottom), and are tabulated in Table 5. As expected, the protonation is favored on the phenolate oxygen atoms, as PA1 is systematically larger than PA2 for all metals. Hence, deprotonation of the donor molecules (MN, ECA) will preferably take place on the phenolate oxygen atoms. The Ni, Co and Zn materials show the largest proton affinity, while Cu behaves somewhat differently in the sense that the basicity of the phenolate oxygen is dramatically reduced, coming closer to that of the carboxylate oxygen atoms. The performance of the Cu material in the experiments also strongly varies depending on the choice of the acidic donor. While the high proton affinity of the phenolate in e.g. $Ni_2$dobdc is consistent with

the high observed activity for this material, it is clearly impossible to rationalize all reactivity trends based on the crude PA values alone. In the following subsection the deprotonation will be examined in the reaction itself, with explicit consideration of the nature of the acidic donor molecule, and of the presence of one or more adjacent open metal sites.

**Table 5.** Proton affinities of $M_2$dobdc at 0 K, for the phenolate oxygen atom (PA1, kJ/mol), and for the carboxylate oxygen atom (PA2, kJ/mol). Also given are the computed adsorption energies of the basic probe molecules acetonitrile and carbon monoxide ($\Delta E_{ads}$, kJ/mol).

| | *M* | PA1 | PA2 | $\Delta E_{ads}(CH_3CN)$ | $\Delta E_{ads}(CO)$ |
|---|---|---|---|---|---|
| *1* | Mg | 930.3 | 912.5 | -91.1 | -44.7 |
| *2* | Co | 947.2 | 918.1 | -82.8 | -92.3 |
| *3* | Ni | 945.5 | 757.3 | -90.7 | -79.0 |
| *4* | Cu | 922.5 | 905.0 | -47.3 | -27.4 |
| *5* | Zn | 944.2 | 917.1 | -78.9 | -38.8 |

Regarding the characteristics of the open metal site, the adsorption energy of some small Lewis basic probe molecules (CO, acetonitrile) on the framework may be used as an indicative factor. In order to quantify the possible roles of *cus* sites in the reactions under scrutiny, the adsorption energies of such probe molecules on the *cus* were studied. Heats for adsorption of CO in $M_2$dobdc materials (M = Ni, Mg, Zn) have been recently calculated by Valenzano et al. [68] using DFT and hybrid MP2/DFT methods. Of these metals, Ni is the one with the largest adsorption energy for CO. Values for Mg and Zn are closer together, but all level of theory methods applied by Valenzano predict the order: Ni > Mg > Zn. For completeness, we also performed adsorption calculations for a larger set of metals. The results are reported in Table 5 and the following trend was found: Co > Ni > Mg > Zn > Cu, in agreement with Valenzano et al. Reported values for the adsorption of CO on $Ni_2$dobdc are remarkably larger than those predicted by Valenzano et al.[68] The high affinity of $Ni_2$dobdc and

$Co_2$dobdc for CO can be rationalized by considering that the *cus* in these materials not only can accept an electron pair, but can also provide $\pi$-backdonation to the CO.[28, 61, 69-71]

Also incorporated in Table 5 are the adsorption energies of acetonitrile on the various $M_2$dobdc materials, as we expect a similar adsorption sequence for the donors with nitrile groups, such as MN or ECA. Inspection of Table 5 learns that the correlation between the two series of adsorption energies, for CO and acetonitrile respectively, is rather poor. In addition the adsorption energies vary over a broad range of values. The most striking case of a different adsorption pattern is offered by the Mg material, with a difference of almost 50 kJ/mol in adsorption energy between acetonitrile and CO. One common feature in the two series of adsorption energies, is the result for Cu, manifesting itself as an outlier in generating low predicted values for the adsorption of the two probe molecules.

Summarizing, the ranking of the metals with respect to the energies of adsorption of Lewis bases seems different for each probe molecule investigated; however, the Ni material, which we selected as a preferred catalyst, invariably shows one of the strongest interactions, irrespective of the nature of the Lewis base. On the other hand, when considered itself as a base, the $Ni_2$dobdc material also displays a considerable PA. Thus, the simulations do not indicate that there would be an inverse relationship between the adsorption energies of probe molecules on the open metal sites, and the basicity of the adjacent framework phenolate. This suggests that one and the same material could contain both active base and reactive open metal sites.

### 3.4.2. Mechanism of basic reactions on the active site and rationalization of activity

We now focus on the reaction steps initiating the Knoevenagel condensation, namely the adsorption of the donor molecule on the metal site, and the subsequent deprotonation on the adjacent phenolate as schematically shown in Figures 5 and 6. We consider two donors, MN and the less acidic ECA, and take into account different adsorption positions of the donors. MN has two nitrile

groups of which just one or two could be adsorbed on neighboring metal sites (Figure 5 (b) and (c)). The energies associated with the different stages are also plotted for the different metals.

The adsorption profiles of MN and ECA with the (nitrile) nitrogen atom adsorbed on the metal (Figure 5 (b) and 6 (b)) resemble each other and are in line with the ranking predicted in the preliminary study with acetonitrile as probe molecule (Table 5). The energies of the deprotonated MN or ECA donor molecules give a different order, which takes into account all intrinsic properties of catalyst and donor molecules (Figure 5(d) and 6(c)). The deprotonation of MN (Figure 5(d)) leads to reaction energies which are slightly negative (exothermic) with respect to the donor in gas phase. For $Ni_2$dodbc, the transition barrier for the deprotonation of MN was determined to be 5.5 kJ/mol with respect to the deprotonated product state. As the energy difference between transition state and deprotonated product is so small, we can assume that the energy levels of the deprotonated products are a good approximation of the deprotonating potential of $Ni_2$dodbc. Provided the deprotonation step of the donor molecule is rate determining for the overall reaction, and is thermodynamically driven, the sequence of the energy levels of the deprotonated product may be regarded as an indicator for the prediction of the ranking of the performance of the various $M_2$dobdc catalysts in the Knoevenagel reaction. For the Knoevenagel condensation of BA and MN on $M_2$dobdc, the agreement is remarkably good, with the overall order of Ni > Cu > Mg ~Zn > Co being reflected in experiment (Table 1) and in theory (Figure 5 (d)).

Another plausible adsorption mode of the MN donor corresponds to a double coordination with two terminating nitrile groups on two adjacent metal sites, which geometrically fits perfectly for MN (Figure 5(c)). As expected, the adsorption energies are lower due to the energetically favorable interaction between the nitrile groups and the metal centers. For instance, in the $Ni_2$dobdc case, the double coordination results in an adsorption energy that is 44.8 kJ/mol more negative than the single coordination. This confirms the hypothesis that an excess of MN could block the coordinatively unsaturated sites, which could play a role in activating the acceptor in Michael additions (see Figure 2

and related discussion). On the other hand, this double adsorption mode is subjected to a larger entropic penalty as more degrees of freedom are immobilized during this step, compensating for a large part the electronic adsorption energies. We performed a frequency calculation for the Ni case, and found free energies of adsorption of -32.2 kJ/mol in case of one adsorption site and -38.1 kJ/mol in case of adsorption of the two nitrile groups at a temperature of 373 K. For the reaction to proceed via deprotonation as in Figure 5(d), one of the coordinations should be lifted, in order to allow the proton hopping to the phenolate oxygen of the framework.

In case of ECA interaction with an active site within $M_2$dobdc, ECA can be adsorbed and deprotonated in two different ways (Figure 6). First, we consider the adsorption of the nitrile group on the metal site, followed by deprotonation. As ECA is less acidic than MN, it is not surprising that a different order of activity is obtained with positive reaction energies (endothermic) for most of the metals, except for Ni (Figure 6(c)). These results are in line with the generally lower conversion rates observed experimentally for reactions with ECA as donor after 2 h of reaction (Table 1). Second, the adsorption of the (carbonyl) oxygen atom on a metal site looks also an attractive pathway, as it results in a more stable adsorption structure (Figure 6(d)). However, after deprotonation, an end product is formed that inhibits further reaction with benzaldehyde. The proton for benzaldehyde adsorption is shielded and the C=C double bond makes the reactive carbon less reactive (see Figure 6(e)). The formation of such a stable, but unreactive intermediate would be in line with the low experimentally observed overall rate for the Knoevenagel reaction between ECA and BA (Table 1).

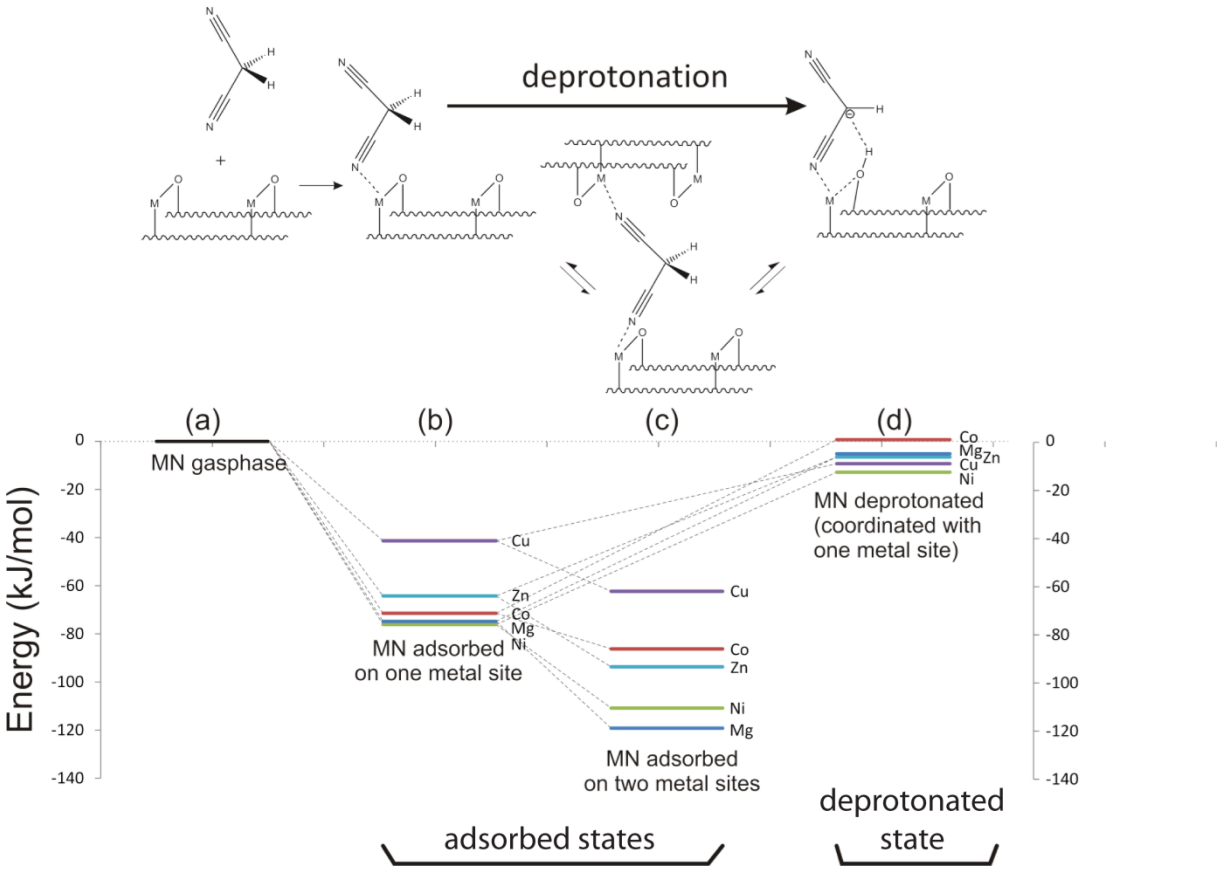


**Figure 5.** Schematic representation of adsorption and subsequent deprotonation reaction of malononitrile (MN), and corresponding energy profiles for different $M_2$dobdc materials. MN can be adsorbed on one (b) or two adjacent metal sites (c). Note that the deprotonation of MN, adsorbed at two metal sites, can only occur if one nitrile-metal coordination is released (d).

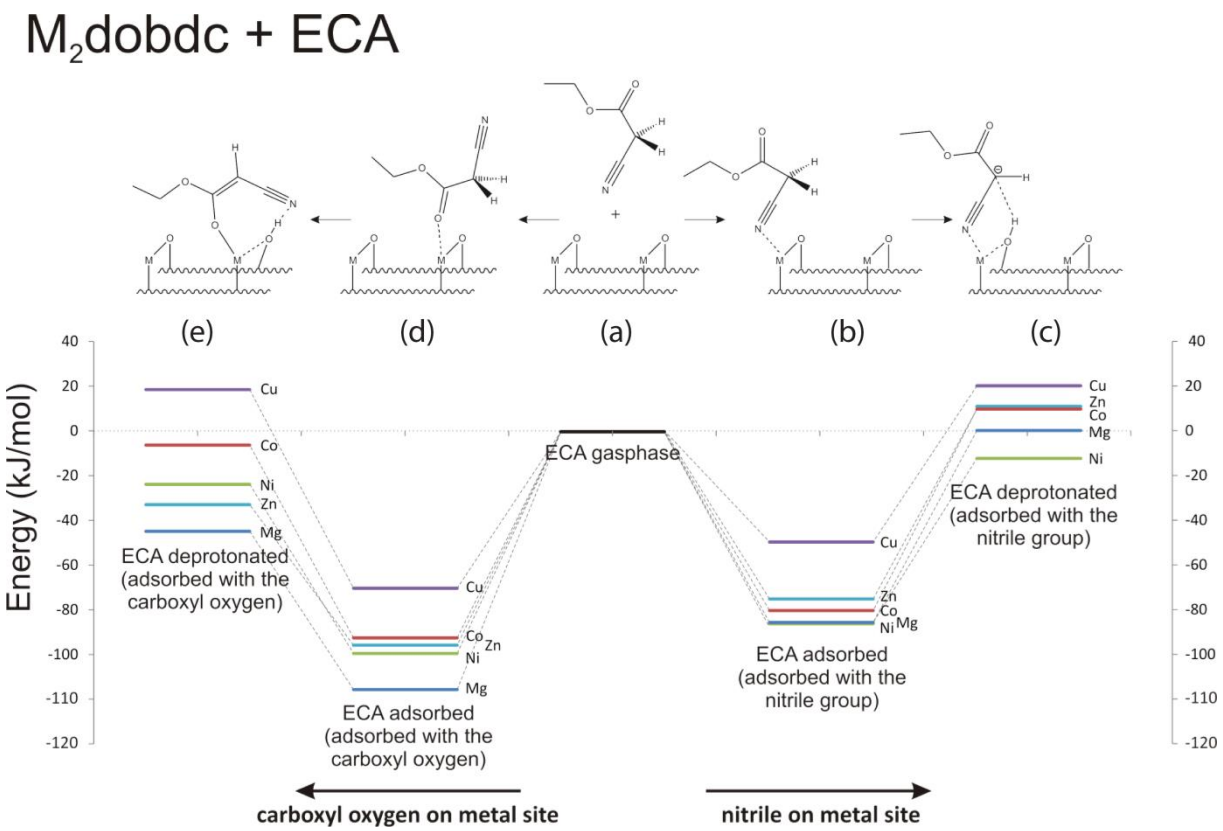


**Figure 6.** Schematic representation of adsorption and subsequent deprotonation reactions of ethyl cyanoacetate (ECA) and corresponding energy profile for different $M_2$dobdc materials. ECA can be adsorbed with the nitrile group (b), but also with the carboxyl oxygen (d). Note that the end product obtained after deprotonation of the adsorbed complex with the carboxyl oxygen coordinated with the metal (e), is not susceptible to further reaction with BA.

It is clear that besides the initial deprotonation and formation of an adsorbed anionic intermediate, other steps in the catalytic cycle, such as C-C coupling and dehydration (Scheme 2) could have their impact on the relative overall rates observed for the various $M_2$dobdc catalysts. However, at least for the Knoevenagel condensations, preliminary calculations have shown that the further condensation of the adsorbed anionic intermediate with BA, as shown in Scheme 2, occurs in an almost barrierless fashion. Hence, for this particular reaction, the subsequent elementary steps will not alter the ranking of activity as extracted from the deprotonation process of the donor adsorbed on the metal site of the framework (Figure 5(d)). For the Michael addition, such firm statements cannot yet be made; deeper understanding may be acquired by modeling explicitly the reaction, likely including the

adsorption of methyl vinyl ketone on a Lewis acid site. Activation of both donor and acceptor will also be affected by the equilibrium concentrations of the reactants in the pores. Such overall computational study falls outside the scope of the present theoretical calculation.

The only deviating case in all simulations is the Cu material, for which the theory systematically predicts high energy intermediates, and hence, a very low reactivity. We have no plausible explanation for this observation. The ground state valence electronic configuration of $Cu^{2+}$ is [Ar] $3d^9$ with one hole in the fully occupied 3d orbital (single electron in the axial $3d_z^2$ orbital). In contrast to $Mg^{2+}$ and $Zn^{2+}$, both exhibiting fully occupied subshells, serious distortions are noticed from the octahedral geometry in the optimized $Cu_2$dobdc unit cell. In the most stable state we have found, the unit cell of $Cu_2$dobdc (containing 36 Cu-atoms) has a total spin of about 1.9, and shows by far the smallest cell volume (Table S.2) with very compressed Cu-Cu distances (3 Å) in the c-direction of the crystal. Probably, the LOT applied to the other $M_2$dobdc materials with success, does not suit the Cu case. In this context the work of Nachtigall [72] on the role of the functional in the prediction of adsorption energies of propane and propylene on the MOF $Cu_3BTC_2$ is of particular interest.

**4. Conclusions**

While the development of metal-organic frameworks as base catalysts has mainly focused on the use of N-functionalized linkers, the use of $M_2$dobdc as a catalyst for Knoevenagel condensation or Michael addition reactions shows that it is possible to use MOFs with an intrinsic basic lattice activity. The catalytic activity of the $M_2$dobdc materials in these reactions can be ascribed to the presence of basic phenolate oxygen atoms in the structure, which, together with the adjacent coordinatively unsaturated metal ions, make up the active site. The nature of the metal ion has been shown to strongly influence the overall activity, and these effects were also investigated computationally. If, at least for the Knoevenagel condensation, the deprotonation of the adsorbed donor molecules is the slowest step, and assuming that this first step is thermodynamically driven, our computations succeed in predicting a correct ranking of the activity for the metals under study. This is remarkable,

since such calculations do not take into account possible fluctuations of the numbers of well accessible active sites in the $M_2$dobdc materials, e.g. due to fault planes or channel obstructions in the crystals. Moreover, due to different adsorption preferences, the intraporous concentrations of the reactants may also vary for the different materials. Finally, the role of the solvent inside the pores was not considered.

There is a clear preference for $Ni_2$dobdc as the generally most active catalyst. The material with Ni at the nodal points combines a clear basic activity, reflected in an energetically favorable deprotonation of $–CH_2$- donor molecules, with sufficiently strong reactant binding open metal sites, accounting for the generally satisfactory catalytic performance displayed by $Ni_2$dobdc.

**5. Acknowledgements**

The authors are grateful to the Belgian Federal Government for support in the IAP project 07/05 Functional Supramolecular Systems, D.V. and P.V. are grateful to K. U. Leuven for the Methusalem CASAS grant, and to FWO Vlaanderen for research project funding G.0453.09 and G.0486.12. P.V. and M.V. are grateful for a fellowship from FWO Vlaanderen. Funding was also received from the European Research Council under FP7 with ERC grant agreement number 240483, the Ghent University and the FWO Vlaanderen. Computational resources and services were provided by Ghent University (Stevin Supercomputer Infrastructure).

**6. References**

[1] J.R. Li, J. Sculley, H.C. Zhou, Chem. Rev., 112 (2012) 869-932.

[2] A. Corma, H. García, F.X. Llabrés i Xamena, Chem. Rev., 110 (2010) 4606-4655.

[3] P. Valvekens, F. Vermoortele, D. De Vos, Catal. Sci. Technol., 3 (2013) 1435-1445.

[4] J. Gascon, U. Aktay, M.D. Hernandez-Alonso, G.P.M. van Klink, F. Kapteijn, J. Catal., 261 (2009) 75-87.

[5] P. Kasinathan, Y.K. Seo, K.E. Shim, Y.K. Hwang, U.H. Lee, D.W. Hwang, D.Y. Hong, S.B. Halligudi, J.S. Chang, Bull. Korean Chem. Soc., 32 (2011) 2073-2075.

[6] M. Savonnet, S. Aguado, U. Ravon, D. Bazer-Bachi, V. Lecocq, N. Bats, C. Pinel, D. Farrusseng, Green Chem., 11 (2009) 1729-1732.

[7] Y. Tan, Z. Fu, J. Zhang, Inorg. Chem. Commun., 14 (2011) 1966-1970.

[8] F.X. Llabrés i Xamena, F.G. Cirujano, A. Corma, Microporous Mesoporous Mater., 157 (2012) 112-117.

[9] U.P.N. Tran, K.K.A. Le, N.T.S. Phan, ACS Catal., 1 (2011) 120-127.

[10] C. Chizallet, S. Lazare, D. Bazer-Bachi, F. Bonnier, V. Lecocq, E. Soyer, A.A. Quoineaud, N. Bats, J. Am. Chem. Soc., 132 (2010) 12365-12377.

[11] L.T.L. Nguyen, K.K.A. Le, H.X. Truong, N.T.S. Phan, Catal. Sci. Technol., 2 (2012) 521-528.

[12] T. Maity, D. Saha, S. Das, S. Koner, Eur. J. Inorg. Chem., 2012 (2012) 4914-4920.

[13] D. Saha, T. Maity, R. Sen, S. Koner, Polyhedron, 43 (2012) 63-70.

[14] D. Saha, R. Sen, T. Maity, S. Koner, Dalton Trans., 41 (2012) 7399-7408.

[15] R. Sen, D. Saha, S. Koner, Chem. Eur. J., 18 (2012) 5979-5986.

[16] P.D.C. Dietzel, Y. Morita, R. Blom, H. Fjellvåg, Angew. Chem., Int. Ed., 44 (2005) 6354-6358.

[17] P.D.C. Dietzel, B. Panella, M. Hirscher, R. Blom, H. Fjellvag, Chem. Commun., (2006) 959-961.

[18] P.D.C. Dietzel, R. Blom, H. Fjellvåg, Eur. J. Inorg. Chem., 2008 (2008) 3624-3632.

[19] P.D.C. Dietzel, R.E. Johnsen, R. Blom, H. Fjellvåg, Chem. Eur. J., 14 (2008) 2389-2397.

[20] W. Zhou, H. Wu, T. Yildirim, J. Am. Chem. Soc., 130 (2008) 15268-15269.

[21] N.L. Rosi, J. Kim, M. Eddaoudi, B. Chen, M. O'Keeffe, O.M. Yaghi, J. Am. Chem. Soc., 127 (2005) 1504-1518.

[22] L. Mitchell, B. Gonzalez-Santiago, J.P.S. Mowat, M.E. Gunn, P. Williamson, N. Acerbi, M.L. Clarke, P.A. Wright, Catal. Sci. Technol., 3 (2013) 606-617.

[23] E.D. Bloch, W.L. Queen, R. Krishna, J.M. Zadrozny, C.M. Brown, J.R. Long, Science, 335 (2012) 1606-1610.

[24] S.J. Geier, J.A. Mason, E.D. Bloch, W.L. Queen, M.R. Hudson, C.M. Brown, J.R. Long, Chem. Sci., 4 (2013) 2054-2061.

[25] D. Britt, H. Furukawa, B. Wang, T.G. Glover, O.M. Yaghi, PNAS, 106 (2009) 20637-20640.

[26] P.D.C. Dietzel, V. Besikiotis, R. Blom, J. Mater. Chem., 19 (2009) 7362-7370.

[27] J. Liu, J. Tian, P.K. Thallapally, B.P. McGrail, J. Phys. Chem. C, 116 (2012) 9575-9581.

[28] E.J. García, J.P.S. Mowat, P.A. Wright, J. Pérez-Pellitero, C. Jallut, G.D. Pirngruber, J. Phys. Chem. C, 116 (2012) 26636-26648.

[29] S.M. Chavan, G.C. Shearer, E. Bloch, S. Bordiga, Chemphyschem, 13 (2012) 445-448.

[30] P.K. Allan, P.S. Wheatley, D. Aldous, M.I. Mohideen, C. Tang, J.A. Hriljac, I.L. Megson, K.W. Chapman, G. De Weireld, S. Vaesen, R.E. Morris, Dalton Trans., 41 (2012) 4060-4066.

[31] T. Remy, S.A. Peter, S. Van der Perre, P. Valvekens, D.E. De Vos, G.V. Baron, J.F.M. Denayer, J. Phys. Chem. C, 117 (2013) 9301-9310.

[32] S. Xiang, W. Zhou, Z. Zhang, M.A. Green, Y. Liu, B. Chen, Angew. Chem., Int. Ed., 49 (2010) 4615-4618.

[33] J.S. Lee, S.B. Halligudi, N.H. Jang, D.W. Hwang, J.S. Chang, Y.K. Hwang, Bull. Korean Chem. Soc., 31 (2010) 1489-1495.

[34] Y. Fu, D. Sun, M. Qin, R. Huang, Z. Li, RSC Adv., 2 (2012) 3309-3314.

[35] S.R. Caskey, A.G. Wong-Foy, A.J. Matzger, J. Am. Chem. Soc., 130 (2008) 10870-10871.

[36] N. Trukhan, U. Muller, A. Panchenko, I. Malkowsky, A. Fischer, Novel metal-organic frameworks as electrode material for lithium ion accumulators, in: World Intellectual Property Organization (Ed.), BASF SE, 2011.

[37] J.L.C. Rowsell, O.M. Yaghi, J. Am. Chem. Soc., 128 (2006) 1304-1315.

[38] G. Kresse, J. Furthmüller, Phys. Rev. B, 54 (1996) 11169-11186.

[39] G. Kresse, J. Furthmüller, Comput. Mater. Sci., 6 (1996) 15-50.

[40] G. Kresse, J. Hafner, Phys. Rev. B, 47 (1993) 558-561.

[41] G. Kresse, J. Hafner, Phys. Rev. B, 49 (1994) 14251-14269.

[42] J.P. Perdew, K. Burke, M. Ernzerhof, Phys. Rev. Lett., 77 (1996) 3865-3868.

[43] J.P. Perdew, K. Burke, M. Ernzerhof, Phys. Rev. Lett., 78 (1997) 1396-1396.

[44] S. Grimme, J. Antony, S. Ehrlich, H. Krieg, J. Chem. Phys., 132 (2010).

[45] P.E. Blöchl, Phys. Rev. B, 50 (1994) 17953-17979.

[46] M.J. Frisch, G.W. Trucks, H.B. Schlegel, G.E. Scuseria, M.A. Robb, J.R. Cheeseman, G. Scalmani, V. Barone, B. Mennucci, G.A. Petersson, H. Nakatsuji, M. Caricato, X. Li, H.P. Hratchian, A.F. Izmaylov, J. Bloino, G. Zheng, J.L. Sonnenberg, M. Hada, M. Ehara, K. Toyota, R. Fukuda, J. Hasegawa, M. Ishida, T. Nakajima, Y. Honda, O. Kitao, H. Nakai, T. Vreven, J.J.A. Montgomery, J.E. Peralta, F. Ogliaro, M. Bearpark, J.J. Heyd, E. Brothers, K.N. Kudin, V.N. Staroverov, R. Kobayashi, J. Normand, K. Raghavachari, A. Rendell, J.C. Burant, S.S. Iyengar, J. Tomasi, M. Cossi, N. Rega, J.M. Millam, M. Klene, J.E. Knox, J.B. Cross, V. Bakken, C. Adamo, J. Jaramillo, R. Gomperts, R.E. Stratmann, O. Yazyev, A.J. Austin, R. Cammi, C. Pomelli, J.W. Ochterski, R.L. Martin, K. Morokuma, V.G. Zakrzewski, G.A. Voth, P. Salvador, J.J. Dannenberg, S. Dapprich, A.D. Daniels, Ö. Farkas, J.B. Foresman, J.V. Ortiz, J. Cioslowski, D. J. Fox, Inc., Wallingford CT, 2009.

[47] A.D. Becke, J. Chem. Phys., 98 (1993) 5648-5652.

[48] C. Lee, W. Yang, R.G. Parr, Phys. Rev. B, 37 (1988) 785-789.

[49] T. Verstraelen, V. Van Speybroeck, M. Waroquier, J. Chem. Inf. Model., 48 (2008) 1530-1541.

[50] A. Ghysels, T. Verstraelen, K. Hemelsoet, M. Waroquier, V. Van Speybroeck, J. Chem. Inf. Model., 50 (2010) 1736-1750.

[51] P. Serra-Crespo, E.V. Ramos-Fernandez, J. Gascon, F. Kapteijn, Chem. Mater., 23 (2011) 2565-2572.

[52] M. Almasi, V. Zelenak, M. Opanasenko, J. Cejka, Dalton Trans., 43 (2014) 3730-3738.

[53] M. Opanasenko, A. Dhakshinamoorthy, J. Čejka, H. Garcia, ChemCatChem, 5 (2013) 1553-1561.

[54] M. Opanasenko, A. Dhakshinamoorthy, M. Shamzhy, P. Nachtigall, M. Horacek, H. Garcia, J. Cejka, Catal. Sci. Technol., 3 (2013) 500-507.

[55] M. Shamzhy, M. Opanasenko, O. Shvets, J. Cejka, Frontiers in Chemistry, 1 (2013).

[56] A. Corma, R.M. Martín-Aranda, J. Catal., 130 (1991) 130-137.

[57] C. Xu, J.K. Bartley, D.I. Enache, D.W. Knight, G.J. Hutchings, Synthesis, 2005 (2005) 3468-3476.

[58] K. Mori, T. Hara, T. Mizugaki, K. Ebitani, K. Kaneda, J. Am. Chem. Soc., 125 (2003) 11460-11461.

[59] A. Coelho, Comb. Chem. High Throughput Screening, 11 (2008) 843.

[60] P.J. Black, M.G. Edwards, J.M.J. Williams, Tetrahedron, 61 (2005) 1363-1374.

[61] L. Valenzano, J.G. Vitillo, S. Chavan, B. Civalleri, F. Bonino, S. Bordiga, C. Lamberti, Catal. Today, 182 (2012) 67-79.

[62] J.C. Lavalley, Catal. Today, 27 (1996) 377-401.

[63] J. Kučera, P. Nachtigall, J. Kotrla, G. Košová, J. Čejka, J. Phys. Chem. B, 108 (2004) 16012-16022.

[64] R.A. Jones, B.G. P., The chemistry of pyrroles, Academic press, New York, 1977.

[65] P.O. Scokart, P.G. Rouxhet, J Chem Soc Faraday T 1, 76 (1980) 1476-1489.

[66] S. Kobayashi, Y. Yamashita, Acc. Chem. Res., 44 (2010) 58-71.

[67] M. Hatano, T. Horibe, K. Ishihara, Angew. Chem., Int. Ed., (2013) 4549-4553.

[68] L. Valenzano, B. Civalleri, K. Sillar, J. Sauer, J. Phys. Chem. C, 115 (2011) 21777-21784.

[69] S. Chavan, F. Bonino, J.G. Vitillo, E. Groppo, C. Lamberti, P.D.C. Dietzel, A. Zecchina, S. Bordiga, Phys. Chem. Chem. Phys., 11 (2009) 9811-9822.

[70] S. Chavan, J.G. Vitillo, E. Groppo, F. Bonino, C. Lamberti, P.D.C. Dietzel, S. Bordiga, J. Phys. Chem. C, 113 (2009) 3292-3299.

[71] L. Valenzano, B. Civalleri, S. Chavan, G.T. Palomino, C.O. Areán, S. Bordiga, J. Phys. Chem. C, 114 (2010) 11185-11191.

[72] M. Rubes, A.D. Wiersum, P.L. Llewellyn, L. Grajciar, O. Bludsky, P. Nachtigall, J. Phys. Chem. C, 117 (2013) 11159-11167.